Title Page

Contribution of extra-hepatic aldehyde oxidase activity to human clearance

Authors:

Kirk D. Kozminski, Jangir Selimkhanov, Scott Heyward, and Michael A. Zientek

Takeda Pharmaceuticals Limited, San Diego, CA (KDK, JS, MAZ)

BioIVT, Baltimore, MD (SH)

Running Title Page

Running title: Contribution of extra-hepatic aldehyde oxidase to clearance

Corresponding author: Kirk D. Kozminski

Address: Takeda Pharmaceuticals Limited, 9625 Towne Centre Drive, San Diego, CA 92121

Tel: 619-930-8239

Email: kirk.kozminski@takeda.com

No. of text pages: 15

No. of tables: 3

No. of figures: 4

No. of references: 39

Abstract word count: 224

Introduction word count: 749

Discussion word count: 1433

Abbreviations: amu, atomic mass unit; AOX, aldehyde oxidase; BW, body weight, CL_{AOX}, total aldehyde oxidase clearance; CL_{int}, intrinsic clearance; CYP, cytochrome P450; DMPK, drug metabolism and pharmacokinetics; FAD, flavin adenine dinucleotide; f_u, fraction unbound; LC/MS/MS, liquid chromatography-tandem mass spectrometry;

Moco, molybdenum pterin cofactor; Q_b, blood flow rate; R_{BP}, blood to plasma

distribution.

Abstract:

Aldehyde oxidase (AOX) is a soluble, cytosolic enzyme that metabolizes various N-heterocyclic compounds and organic aldehydes. It has wide tissue distribution with highest levels found in liver, kidney, and lung. Human clearance projections of AOX substrates by in vitro assessments in isolated liver fractions (cytosol, S9) and even hepatocytes have been largely under-predictive of clinical outcomes. Various hypotheses have been suggested as to why this is the case. One explanation is that extra-hepatic AOX expression contributes measurably to AOX clearance and is at least partially responsible for the often observed under-predictions. Although AOX expression has been confirmed in several extra-hepatic tissues, activities therein and potential contribution to overall human clearance have not been thoroughly studied. In this work, the AOX enzyme activity using the S9 fractions of select extra-hepatic human tissues (kidney, lung, vasculature, and intestine) were measured using carbazeran as a probe substrate. Measured activities were scaled to a whole-body clearance using best-available parameters and compared to liver S9 fractions. Here, the combined scaled AOX clearance obtained from the kidney, lung, vasculature and intestine is very low and amounted to <1% of liver. This work suggests that AOX metabolism from extra-hepatic sources plays little role in the underprediction of activity in human. One of the notable outcomes of this work has been the first direct demonstration of AOX activity in human vasculature.

SIGNIFICANCE STATEMENT

This work demonstrates AOX activity is measurable in a variety of extra-hepatic human tissues, including vasculature, yet activities and potential contributions to human clearance are relatively low and insignificant when compared to the liver. Additionally, the modeling of the tissue specific in vitro kinetic data suggests that AOX may be influenced by the tissue it resides in and thus show different affinity, activity, and modified activity over time.

Introduction

Aldehyde oxidase is a molybdenum cofactor-containing cytosolic enzyme recognized for its potential to oxidize various nitrogen-containing heterocyclic compounds and organic aldehydes (Beedham, 2001; Kitamura et al., 2006; Garattini et al., 2008; Pryde et al., 2010; Terao et al., 2016; Rashidi and Soltani, 2017). Catalytically, the mechanism involves nucleophilic attack at an electron-deficient carbon and insertion of oxygen from water. Apart from oxidation reactions, research shows that AOX could also act as a reductase toward N-oxides, sulfoxides and heterocycles under hypoxic conditions (Kitamura and Tatsumi, 1984a; Kitamura and Tatsumi, 1984b). It has also been demonstrated more recently that AOX can catalyze the hydrolysis of amide bonds (Sodhi et al., 2015).

Interest in AOX has increased considerably in recent years, and DMPK laboratories have implemented assays to screen for its activity. This interest primarily stems from changing chemical-derivation or synthesis trends that, while improving drug properties, may result in clearance by non-CYP pathways. Thus, while introduction of groups such as azaheterocycles may improve log P, solubility and overall CYP liabilities, it may also increase potential for AOX-mediated metabolism. Carbazeran (Kaye et al., 1984), zoniporide (Dalvie et al., 2010), SGX523 (Diamond et al., 2010), and Lu AF09535 (Jensen et al., 2017) are examples of drug candidates that failed clinically as a result of unexpected poor pharmacokinetics or toxic metabolite formation due in part to aldehyde oxidase.

AOX-mediated metabolism can be readily captured in vitro through the use of human cytosolic and S9 liver fractions. Where AOX activity is suspected, confidence can be increased through co-incubation of test substrates with an AOX-specific inhibitor, such as hydralazine (Strelevitz et al., 2012). Though AOX-mediated metabolism can be correctly identified pre-clinically, the clearance in human has generally been under-predicted by in vitro assays, and sometimes quite substantially. A number of estimates suggest the in vitro to in vivo correlation (IVIVC) under-

6

prediction of $CL_{int,in\ vivo}$ could be as much as 10-fold on average for AOX substrates, when plasma protein binding is taken into account (Zientek et al., 2010; Akabane et al., 2012; Hutzler et al., 2013; De Sousa Mendes et al., 2020). Various explanations have been offered in the literature as to why this may be the case, and these include possible loss of enzyme activity during tissue collection and preservation and/or a loss of enzyme activity over the time course of an in vitro assay. Regarding the latter, it has recently been proposed that regeneration of the AOX enzyme in vitro may be rate-limited by flow of electrons from the molybdenum pterin cofactor (MoCo) to the flavin adenine dinucleotide (FAD) for the reduction of oxygen (Abbasi et al., 2019). In that work, the authors proposed a modulated activity model to capture the early fast-rate of the enzyme to improve clearance predictions. However, even with this model, some residual under-prediction persists. Another possibility, often speculated in the literature, is that contributions to AOX metabolism from extra-hepatic tissue could be a key factor in the underpredictions. Immunohistochemical studies have shown that AOX is broadly distributed throughout the human body (Moriwaki et al., 2001). The kidneys, adrenal glands, lungs and reproductive tissue are rich sources, amongst other tissues. A more recent study has confirmed the presence and activity of AOX in human skin (Manevski et al., 2014). While there is no current evidence suggesting that AOX metabolism at any one organ or tissue bed could rival that occurring at the liver, it cannot be ruled out that the collective contributions of many compartments could be significant.

Our objective in this current work was to measure the rates of AOX activity in the S9 fractions from various extra-hepatic tissues known or suspected to express the AOX enzyme and to use best-available physiological parameters to estimate potential contributions to total human AOX clearance. Studies were conducted using carbazeran as a probe substrate, a classic example of a compound with human clearance that is significantly underpredicted by liver tissue fractions. In this work, carbazeran is an ideal tool due to its high intrinsic activity, and although it

7

has been observed to undergo glucuronidation in hepatocytes (Sharma et al., 2012), it is metabolized exclusively by AOX to a single product, 4-oxo-carbazeran in human cytosol, or S9 without cofactors (Kaye et al., 1985; Xie et al., 2019) (**Figure 1**).

While we cannot capture AOX activity in every extra-hepatic tissue compartment, the exercise does reveal the potential significance of extra-hepatic contribution to the overall human AOX clearance of a drug and the collective role AOX containing extra-hepatic tissue may play in the often-observed underprediction phenomenon.

Materials and Methods

Materials

The human vasculature S9 fractions, obtained as a gift from BioIVT (Baltimore, MD), were prepared from the interior linings of iliac arteries collected during standard liver harvesting. The yield of vascular S9 per weight of tissue was calculated from the total protein yielded from the preparation as measured by the BCA protein assay (Thermo Fisher Scientific, Rockford, IL) divided by the weight of tissue used in the preparation, and this is represented as the average of three donors (one male and two females). The human kidney (whole kidney, mixed sex, pool of 8), lung (non-smoker, mixed sex, pool of 4) and intestinal (duodenal and jejunal, prepared by elution, mixed sex, pool of 15) S9 fractions were procured from XenoTech (Kansas City, KS). Human liver S9 fractions were procured from BioIVT (mixed sex, pool of 150). Carbazeran and 4-oxo-carbazeran were procured from Toronto Research Chemicals (ON, Canada), and hydralazine was procured from Sigma Aldrich (St. Louis, MO). Dialysis membranes (6-8 kDa molecular weight cut-off) for protein binding were procured from HTDialysis (Gales Ferry, CT). Water and acetonitrile were of HPLC grade and were procured from Fisher Scientific (Fair Lawn, NJ). All other reagents used in the study were of extra-pure grade.

Methods

Tissue S9 Incubations. Each tissue-specific extra-hepatic S9 fraction (kidney, lung, vasculature, intestinal) was incubated at a final protein concentration of 1 mg/mL in phosphate buffer (100 mM, pH 7.4) with 1, 3, 10 and 30 µM carbazeran. Liver S9 fraction was incubated at a final protein concentration of 0.1 mg/mL in an identical manner. The lower end of the carbazeran concentration range (1 µM) was chosen specifically to represent concentrations

9

lower than the Michaelis-Menten constant (K_M) values reported in the literature (3-6 µM), and assumed to provide the highest rate of metabolite formation (Chen et al., 2019; Tan et al., 2020; Uehara et al., 2020). Thus, the lower end of the concentrations range is assumed to provide an accurate account of maximum CL_{int} (~V_{max}/K_M). Pooled S9 products were incubated in duplicate (lung, kidney, intestinal) or triplicate (liver) at each substrate concentration. For vasculature S9, each individual donor was tested separately at each test concentration. No cofactors were added to any incubations. Incubations (300 µL starting volume) were conducted in 96 deep well plates (Thomson Instruments, Oceanside, CA) using a Thermomixer (Eppendorf, Hamburg, Germany) at 37 °C with a shaking speed of 600 rpm. Aliquots (30 µL) were removed at 0, 3, 7, 15, 30, 60 and 90 minutes post incubation and quenched with 200 µL of chilled acetonitrile containing a proprietary internal standard. Parallel incubations were conducted in the presence of hydralazine (100 µM final concentration), a known AOX inhibitor. All collected samples were centrifuged at 4000 x g for 10 minutes, and supernatants were diluted 3-fold in water prior to LC/MS/MS injection. Authentic standards of 4-oxo-carbazeran were prepared in the non-fortified S9 tissue matrices and processed in an identical manner.

Protein Binding. The protein binding assay for extra-hepatic S9 fractions was conducted using equilibrium dialysis. Tissue-specific S9 fractions (1 mg/mL protein) fortified with 1 µM compound and blank 100 mM phosphate buffer, pH 7.4 were placed on opposite sides of a divided 96-well dialysis membrane device. Samples (triplicates) were dialyzed against buffer for a total of 6 hr at 37 °C and 5% CO_2 on an oscillating platform inside a standard cell culture incubator. At the end of the incubation period, donor and receiver samples were matrix matched (10 µL of S9 study sample and 40 µL of blank assay buffer, or 40 µL of buffer study sample and 10 µL of non-fortified S9 matrix) and were quenched with 200 µL of chilled acetonitrile containing a proprietary internal standard. Quenched samples were centrifuged at

4000 x g for 10 minutes, and supernatants were diluted 3-fold in water prior to LC/MS/MS injection.

LC/MS/MS Analysis.   Analysis was conducted with an API4500 triple quadrupole mass spectrometer (AB Sciex, Ontario, Canada). Samples were analyzed with electrospray ionization in the positive mode with a source temperature of 500 °C. The parent > daughter transition monitored for carbazeran was 361.2 > 218.1 amu, and the collision energy was set at 38 volts. The parent > daughter transition monitored for 4-oxo-carbazeran was 377.1 > 288.1 amu, and the collision energy was set at 23 volts. The HPLC column (Kinetex C18-XB, 50 x 2.1 mm, 5 µm particles) was procured from Phenomenex (Torrance, CA). The mobile phase consisted of HPLC-grade water with 0.1% formic acid and acetonitrile with 0.1% formic acid for components A and B, respectively. The mobile phase was held at 5% B and ramped to 95% B over 1.3 minutes at a flow rate of 0.6 mL/min. The total run time was 1.5 minutes. LC/MS/MS chromatograms were collected and integrated with Analyst software (version 1.6). A standard curve (1-500 nM) was used to quantify 4-oxo-carbazeran formation in all extra-hepatic S9 study samples (kidney, lung, vasculature, intestinal). For liver S9 study samples, the standard curve range was shifted up to 8-fold higher (8-4000 nM), depending on substrate incubation concentration, to capture the higher amounts of metabolite formed in these incubations. Assay performance was accepted based on linearity throughout the dynamic range of the curve (R >0.99 with $1/x^2$ weighting) and back-calculation of standards to within 20% of the nominal value.

Data Analysis. Consistent with supporting data acquired during the studies presented within this manuscript, the AOX pathway was presumed to be the only pathway contributing to carbazeran clearance utilizing S9 tissue fractions, with 4-oxo-carbazeran being the sole metabolite formed. As such, carbazeran intrinsic clearance (CL_{int}) in each tissue was estimated based on 4-oxo-carbazeran time-course data obtained in the various S9 incubations, and calculated according to

$$CL_{int} = \frac{V_{max,tissue}}{K_{M,tissue}} \quad \text{(Equation 1)}$$

In Equation 1, AOX maximum 4-oxo-carbazeran formation rate ($V_{max,tissue} = E_{tissue} \times k_{cat,fast}$) and Michaelis-Menten constant ($K_{M,tissue} = \frac{k_{on}+k_{cat,fast}}{k_{off,tissue}}$) were calculated using parameters of AOX modulated activity model (Abbasi et al., 2019), which were estimated by fitting the model (**Figure 2**) to the 4-oxo-carbazeran time-course data. In the model, $k_{cat,fast}$ is the initial fast AOX catalytic rate constant, E_{tissue} is the initial active AOX concentration in each of the tissues, k_{on} is the binding rate constant, and $k_{off,tissue}$ is the tissue-specific unbinding rate constant. The model was implemented in MATLAB R2019 (MathWorks, Natick, MA) and simultaneously fit to 4-oxo-carbazeran mean concentration time-course data from all tissue S9 incubations using default fitnlm algorithm settings with a proportional error model and all model parameters assumed to be log-normally distributed. Description of the full model characterization can be found in the Supplementary Materials.

The CL$_{int}$ values were scaled to in vivo (CL$_{int,scaled}$) for each tissue according to

$$CL_{int,scaled} = CL_{int} * \frac{mg\ S9\ protein}{g\ tissue} * \frac{g\ tissue}{kg\ body\ wt} \quad \text{(Equation 2)}$$

Total AOX clearance (CL$_{AOX}$) contributions from liver, kidney, lung and intestinal compartments were estimated by the well-stirred model as follows:

$$CL_{AOX} = \frac{Q_b * \left(f_{u,plasma}/R_{BP}\right) * \left(CL_{int,scaled}/f_{u,S9}\right)}{Q_b + \left(f_{u,plasma}/R_{BP}\right) * \left(CL_{int,scaled}/f_{u,S9}\right)} \quad \text{(Equation 3)}$$

where Q$_b$ is blood flow to the tissue compartment, f$_{u,plasma}$ is unbound free fraction in plasma, R$_{BP}$ is the blood-to-plasma concentration distribution, and f$_{u,S9}$ is the free fraction in the S9

incubations. For vasculature, it was considered that there is continuous exposure to the blood throughout the body, and the blood flow restriction was removed. Furthermore, it was assumed that the iliac arterial tissue was representative of the entirety of the human vasculature. CL_{AOX} from the vasculature was estimated as follows:

$$CL_{AOX} = \left(\frac{f_{u,plasma}}{R_{BP}}\right) * \left(\frac{CL_{int,scaled}}{f_{u,S9}}\right) \quad \text{(Equation 4)}$$

All physiological parameter values used in the above equations are recorded in Table 1. The $f_{u,plasma}$ and R_{BP} values for carbazeran, 0.08 and 0.7, respectively, were taken from a previous publication (Zientek et al., 2010). Carbazeran $f_{u,S9}$ was measured by equilibrium dialysis and determined to be 0.72, 0.82, 0.72 and 0.74 for kidney, lung, vasculature and intestinal S9 fractions (1 mg/mL), respectively. For the liver S9 fraction (0.1 mg/mL), carbazeran consumption by AOX is too extensive to measure binding by equilibrium dialysis. Here, liver $f_{u,S9}$ was calculated as 0.97 per the non-specific binding model (Austin et al., 2002) as follows:

$$f_{u,liverS9} = \frac{1}{\left(\frac{[P]_{extra-hepaticS9}}{[P]_{liverS9}} * \left(\frac{1 - f_{u,extra-hepaticS9}}{f_{u,extra-hepaticS9}}\right) + 1\right)} \quad (Equation\ 5)$$

where $[P]_{extra-hepaticS9}$ is 1 mg/mL, $[P]_{liverS9}$ is 0.1 mg/mL, and $f_{u,extra-hepaticS9}$ is 0.75, which is the average f_u measured across all extra-hepatic tissues (kidney, lung, vasculature, intestinal) studied.

13

Results

Following the in vitro incubations with carbazeran, non-linear formation of 4-oxo-carbazeran metabolite was observed and quantified against authentic standards in the liver, kidney, lung and vasculature S9 fractions at all incubation concentrations (**Figure 3a, b, c, d, e, respectively**). Across all incubations, initial faster rate of 4-oxo-carbazeran formation was quickly followed by a slower rate of formation. Only negligible amounts of metabolite were detected in the intestinal S9 fractions, and specifically only observed at the higher incubation concentrations (**Figure 3f**) and associated with the slower rate of formation. While the extent of carbazeran elimination was too low to be accurately measured in extra-hepatic S9 fractions, it was easily observed in liver S9 fractions, and there was an approximate mass balance between substrate consumption and metabolite formation. A representative plot of carbazeran consumption versus 4-oxo-carbazeran formation for 1 μM incubations in liver S9 fraction is shown in **Figure 3a**. Co-incubation of carbazeran with 100 μM hydralazine, a selective mechanism-based inhibitor of AOX, significantly blocked metabolite formation in all incubations. In liver S9, there was a 93% decrease in metabolite formation at the highest test concentration (30 μM) of carbazeran. Similarly, all extra-hepatic tissues showed at least 81% decrease in metabolite formation at the same conditions. Relative concentrations of 4-oxo-carbazeran quantified at the end of the incubation period (90 minutes) for all carbazeran test concentrations, with and without presence of hydralazine, are presented in **Figure 4** for each tissue S9 fraction tested. Taken together, observed data in human S9 fractions without co-factors suggests that carbazeran is metabolized to a single product, 4-oxo-carbazeran, and this is mediated by the AOX pathway.

14

Despite minimal consumption of carbazeran by the various extra-hepatic tissue S9 samples, 4-oxo-carbazeran metabolite formation quickly followed non-linear kinetics that can be described by the AOX modulated activity model (Abbasi et al., 2019). This model was able to accurately capture (adj. R^2 = 0.99) 4-oxo-carbazeran formation time-course data in all tissue S9 incubations (**Figure 3**), with estimated parameter values captured in Table 2. In the final model, liver and kidney were found to have a lower Michaelis-Menten constant value (5.2 μM) relative to the other tissues (21 μM), as well as different enzyme inactivation and slow catalytic rate constant values (Table 3). In order to estimate intestinal S9 CL_{int} (0.038 μL/min/mg S9) despite minimal 4-oxo-carbazeran formation, it was necessary to assume that the intestinal AOX enzyme rate constants were the same as in other tissue's S9 fractions (lung and vasculature). Similarly, to estimate active AOX enzyme level in each tissue (E_{tissue}), it was assume that the AOX fast catalytic rate constant was the same across all tissues. Thus, we determined that the liver has the highest estimated AOX enzyme concentration level at 21 pmol/mg S9 protein (Table 2). AOX intrinsic clearance estimates, calculated according to Equation 1, were 670, 1.2, 0.35, 0.58, 0.038 μL/min/mg, respectively, for liver, kidney, lung, vasculature, and intestine S9 fractions incubated with carbazeran (Table 3). The scaled intrinsic clearance ($CL_{int,scaled}$) and total AOX clearance (CL_{AOX}) the values estimated in various extra-hepatic tissues were very low relative to the liver (Table 3). Collectively, CL_{AOX} estimates in the extra-hepatic tissues sampled in this current work represent <1% compared to that of the liver.

Discussion

While the human liver is the richest source of AOX, the current study has demonstrated that AOX activity is clearly present and measurable in a variety of extra-hepatic human tissues. Of significance, we demonstrate for the first time that AOX activity is measurable in the human vasculature, as represented by S9 fractions prepared from iliac arteries. Given that AOX has been found to be expressed in a variety of extra-hepatic human tissues beyond the scope of this current work (adrenal glands, reproductive tissue, adipose), it can be fully expected that measurable extra-hepatic AOX activity can be found throughout the human body, which would further contribute to the metabolism of AOX substrates.

Given this backdrop, it seems plausible that the collective contributions to AOX metabolism by extra-hepatic sources could, at a minimum, partially explain the underprediction of human clearance scaled from in vitro assays conducted with pooled hepatic S9 or cytosolic fractions. Admittedly, various assumptions were made in the current study when estimating a potential CL_{AOX} contribution from a particular tissue compartment, and physiological parameters may not be as accurate as those commonly used for liver tissue scaling. Regardless, these assumptions likely have little impact on the overall findings presented in this study, where the extra-hepatic tissues only provide a minor contribution to overall systemic clearance. Here, the collective estimated CL_{AOX} of kidney, lung, vasculature and intestinal compartments together contribute <1% of that predicted by the liver.

The tissue fractions tested were chosen due to the identified expression levels of AOX in the tissue (Basit et al., 2020), the volume of tissue of the organ (Davies and Morris, 1993), and/or

16

the lack of blood flow restriction pertaining to the tissue. While it would have been desirable to study additional human tissues beyond the scope of this work, it is unlikely, based on these criteria that any would contribute significantly to whole-body AOX clearance. For example, the adrenal glands are often cited as having rich AOX expression (Moriwaki et al., 2001; Gomez-Sanchez, 2007). However, adrenal glands are very small, and the combined weight of adult human adrenal glands is only roughly 10 grams (Kreiner, 1982). While adrenal glands may have a rich blood supply on a per gram basis, total blood flow has been estimated at roughly 0.14% of cardiac output (Gomez-Sanchez, 2007), or what would amount to approximately 0.1 mL/min/kg. Similarly, contribution of human skin, which was demonstrated to have limited AOX activity (Manevski et al., 2014), to whole-body AOX clearance would also be insignificant when compared to liver.

Carbazeran, a PDE-1 inhibitor that produces concentration-dependent positive inotropic responses, known for its greater than or equal to hepatic blood flow systemic clearance (≥ 21 ml/min/kg), and being extensively metabolized to the 4-oxo-metabolite in vivo, was chosen as an ideal probe substrate to identify AOX activity in tissue S9 fractions. Carbazeran is also known for its specificity for AOX versus other enzymes in S9 fractions, especially since enzymes that require cofactors in vitro (i.e. UGTs and CYPs) are of little consequence without addition of cofactors, which were excluded from the protocol. Additionally, and perhaps most importantly to these experiments, carbazeran exhibits a rapid turnover rate providing its sensitivity as a marker even with very low AOX expression levels in tissue. Due to this fact, the number of potential substrates available to assess extra-hepatic AOX activity was limited. In addition to carbazeran, zoniporide was tested during the course of these experiments using all of the aforementioned tissues. With protein concentrations up to 1 mg/ml, zoniporide did not result in adequate substrate turnover, even at enzyme saturating substrate concentrations (30 µM), and failed to provide measurable metabolite formation rates, thus disqualifying it as an applicable substrate (**Supplemental Figure 3**).

17

The analysis of the data and scaling of organ specific AOX clearance utilized the well-stirred model. This particular model, as opposed to the dispersion model or parallel tube model, was used because it presents the highest possible in vivo clearance estimate for each tissue's contribution to the overall systemic clearance in humans. For vasculature, the blood flow restriction was removed entirely. Therefore, the possibility of an under-prediction based on the scaling method has been minimized . An interesting observation of this work is that, in all extra-hepatic tissues studied, was the initial rate of 4-oxo-carbazeran production was followed by a rapid deceleration in product formation despite minimal consumption of carbazeran. It has been hypothesized by Abbasi and co-workers that AOX is likely slow to reduce oxygen in vitro, resulting in enzyme reduction that leads to the decelerated substrate turnover. We employed an AOX modulated activity model (Abbasi et al., 2019) in order to accurately capture the early rapid-rate of AOX activity, characterized by the fast catalytic rate constant. Since the early rapid rate of AOX activity in vitro is believed to most accurately represent in vivo AOX activity, the application of the AOX modulated activity model provided us with a more accurate estimate of intrinsic clearance. Despite the more accurate estimate of the initial faster rate of substrate turnover, extra-hepatic AOX contribution estimates were found to be very low.

By assuming that the AOX fast catalytic rate constant is the same across all tissues, the difference in AOX activity between various tissues, as determined by the early rapid-rate of 4-oxo-carbazeran formation, can be attributed to the abundance of active AOX enzyme in S9 fractions. Thus, using the AOX modulated activity model, estimates of active AOX enzyme abundance in each tissue's S9 fraction were obtained. It was found that the active AOX abundance in the liver (21 pmol/mg S9 protein) is in general agreement with measured liver AOX abundance (11.96+/-4.46 pmol/mg S9 protein) described by Basit and colleagues (Basit et al., 2020). In addition, the published extra-hepatic AOX abundance levels for the heart and intestine were below the limit of quantification, which agrees with much lower estimated active AOX levels that we obtained using AOX activity (Table 2). In contrast, Basit et al., 2020 showed

18

only an 8-fold difference in AOX abundance between kidney (1.53+/-0.79 pmol/mg S9 protein) and liver, while our analysis of AOX activity data showed greater than 500-fold reduction in active kidney AOX abundance (0.038 pmol/mg S9 protein) relative to liver. Since enzyme abundance does not always correlate with activity, it is possible that our assumption of tissue-independent enzyme fast catalytic rate is incorrect, which could explain the observed disconnect. Tissue sample preparation differences among suppliers and laboratories, and perhaps between tissues, could also impact the resulting AOX activity and thus the model-derived active AOX enzyme tissue abundance estimates.

In support of potential differences in enzyme activity between tissues, it was necessary to introduce tissue-specific differences in several of the model's enzyme rate constants in order to accurately describe the full 4-oxo-carbazeran time-course data in kidney and liver S9 fractions (Supplementary Material). This observation suggests that it is possible that AOX enzyme activity could be different in various tissues and thus complicates the total metabolic clearance extrapolation based on a recombinant protein enzyme activity and tissue enzyme abundance levels as proposed by Basit et al., 2020. It is possible that sample differences between liver, kidney, and other tissues could have affected observed 4-oxo-carbazeran formation, which would impact interpretation of model-derived active AOX enzyme tissue abundance estimates.

This work suggests that future efforts may be best directed toward understanding aspects of tissue isolation and fraction preparation which may negatively impact AOX activity. Sanoh and co-workers, who isolated human hepatocytes from humanized PXB mice, and then used them to predict human $CL_{int,in\ vivo}$, showed a three-fold or greater under-prediction from the line of unity (Sanoh et al., 2012). This direct comparison of in vivo clearance in humanized mice and the scaled hepatic clearance from hepatocytes, isolated from the same animal, suggests that the loss in AOX activity during preparation of liver cells and fractions may impact our ability to predict human in vivo AOX clearance. Furthermore, despite accounting for the lack of the active AOX enzyme regeneration during the experiment through the modulated activity model,

19

unaccounted factors may affect the level of active AOX enzyme prior to the incubation. Perhaps additional systematic work pertaining to the complexity of enzyme activation may shed more light on the limited enzymatic activity of tissue isolates and ways to correct for it.

In conclusion, this work advances the narrative that AOX is active and measurable in a variety of extra-hepatic human tissues, including the vasculature. However, the collective contribution of the tissues tested in these experiments to whole-body clearance of AOX substrates is very low compared to the liver and are unlikely to contribute significantly toward the often-observed underprediction of human AOX clearance.

Authorship Contributions

Participated in research design: Kozminski and Zientek

Conducted experiments: Kozminski

Performed data analysis: Kozminski and Selimkhanov

Wrote or contributed to the writing of the manuscript: Kozminski, Selimkhanov, Heyward, and

Zientek

21

References

Abbasi A, Paragas EM, Joswig-Jones CA, Rodgers JT, and Jones JP (2019) Time Course of Aldehyde Oxidase and Why It Is Nonlinear. *Drug Metab Dispos* **47:**473-483.

Aird WC (2005) Spatial and temporal dynamics of the endothelium. *J Thromb Haemost* **3:**1392-1406.

Akabane T, Gerst N, Masters JN, and Tamura K (2012) A quantitative approach to hepatic clearance prediction of metabolism by aldehyde oxidase using custom pooled hepatocytes. *Xenobiotica* **42:**863-871.

Austin RP, Barton P, Cockroft SL, Wenlock MC, and Riley RJ (2002) The influence of nonspecific microsomal binding on apparent intrinsic clearance, and its prediction from physicochemical properties. *Drug Metab Dispos* **30:**1497-1503.

Basit A, Neradugomma NK, Wolford C, Fan PW, Murray B, Takahashi RH, Khojasteh SC, Smith BJ, Heyward S, Totah RA, Kelly EJ, and Prasad B (2020) Characterization of Differential Tissue Abundance of Major Non-CYP Enzymes in Human. *Mol Pharm* **17:**4114-4124.

Beedham C (2001) Molybdenum Hydroxylases, in: *Enzyme Systems that Metabolise Drugs and other Xenobiotics* (Ioannides C ed), pp 576, Wiley-VCH.

Chen S, Austin-Muttitt K, Zhang LH, Mullins JGL, and Lau AJ (2019) In Vitro and In Silico Analyses of the Inhibition of Human Aldehyde Oxidase by Bazedoxifene, Lasofoxifene, and Structural Analogues. *J Pharmacol Exp Ther* **371:**75-86.

Cubitt HE, Houston JB, and Galetin A (2011) Prediction of human drug clearance by multiple metabolic pathways: integration of hepatic and intestinal microsomal and cytosolic data. *Drug Metab Dispos* **39:**864-873.

Dalvie D, Zhang C, Chen W, Smolarek T, Obach RS, and Loi CM (2010) Cross-species comparison of the metabolism and excretion of zoniporide: contribution of aldehyde oxidase to interspecies differences. *Drug Metab Dispos* **38:**641-654.

Davies B and Morris T (1993) Physiological parameters in laboratory animals and humans. *Pharm Res* **10:**1093-1095.

De Sousa Mendes M, A LO, Humphries HE, Jones B, Gardner I, Neuhoff S, and Pilla Reddy V (2020) A Laboratory-Specific Scaling Factor to Predict the In Vivo Human Clearance of Aldehyde Oxidase Substrates. *Drug Metab Dispos* **48:**1231-1238.

Diamond S, Boer J, Maduskuie TP, Jr., Falahatpisheh N, Li Y, and Yeleswaram S (2010) Species-specific metabolism of SGX523 by aldehyde oxidase and the toxicological implications. *Drug Metab Dispos* **38:**1277-1285.

Garattini E, Fratelli M, and Terao M (2008) Mammalian aldehyde oxidases: genetics, evolution and biochemistry. *Cell Mol Life Sci* **65:**1019-1048.

Gomez-Sanchez CE (2007) Regulation of adrenal arterial tone by adrenocorticotropin: the plot thickens. *Endocrinology* **148:**3566-3568.

Hutzler JM, Obach RS, Dalvie D, and Zientek MA (2013) Strategies for a comprehensive understanding of metabolism by aldehyde oxidase. *Expert Opin Drug Metab Toxicol* **9:**153-168.

Jensen KG, Jacobsen AM, Bundgaard C, Nilausen DO, Thale Z, Chandrasena G, and Jorgensen M (2017) Lack of Exposure in a First-in-Man Study Due to Aldehyde Oxidase Metabolism: Investigated by Use of 14C-microdose, Humanized Mice, Monkey Pharmacokinetics, and In Vitro Methods. *Drug Metab Dispos* **45:**68-75.

Kaye B, Offerman JL, Reid JL, Elliott HL, and Hillis WS (1984) A species difference in the presystemic metabolism of carbazeran in dog and man. *Xenobiotica* **14:**935-945.

Kaye B, Rance DJ, and Waring L (1985) Oxidative metabolism of carbazeran in vitro by liver cytosol of baboon and man. *Xenobiotica* **15:**237-242.

Kitamura S, Sugihara K, and Ohta S (2006) Drug-metabolizing ability of molybdenum hydroxylases. *Drug Metab Pharmacokinet* **21:**83-98.

Kitamura S and Tatsumi K (1984a) Involvement of liver aldehyde oxidase in the reduction of nicotinamide N-oxide. *Biochem Biophys Res Commun* **120:**602-606.

Kitamura S and Tatsumi K (1984b) Reduction of tertiary amine N-oxides by liver preparations: function of aldehyde oxidase as a major N-oxide reductase. *Biochem Biophys Res Commun* **121:**749-754.

Kreiner E (1982) Weight and shape of the human adrenal medulla in various age groups. *Virchows Arch A Pathol Anat Histol* **397:**7-15.

Levitzky M (2013) *Pulmonary Physiology*. McGraw-Hill Companies, New York, NY.

Manevski N, Balavenkatraman KK, Bertschi B, Swart P, Walles M, Camenisch G, Schiller H, Kretz O, Ling B, Wettstein R, Schaefer DJ, Pognan F, Wolf A, and Litherland K (2014) Aldehyde oxidase activity in fresh human skin. *Drug Metab Dispos* **42:**2049-2057.

Moriwaki Y, Yamamoto T, Takahashi S, Tsutsumi Z, and Hada T (2001) Widespread cellular distribution of aldehyde oxidase in human tissues found by immunohistochemistry staining. *Histol Histopathol* **16:**745-753.

Myers JN, Gujja P, Neelagaru S, Hsu L, and Burkhoff D (2011) Noninvasive measurement of cardiac performance in recovery from exercise in heart failure patients. *Clinics (Sao Paulo)* **66:**649-656.

Obach RS, Walsky RL, Venkatakrishnan K, Gaman EA, Houston JB, and Tremaine LM (2006) The utility of in vitro cytochrome P450 inhibition data in the prediction of drug-drug interactions. *J Pharmacol Exp Ther* **316:**336-348.

Pryde DC, Dalvie D, Hu Q, Jones P, Obach RS, and Tran TD (2010) Aldehyde oxidase: an enzyme of emerging importance in drug discovery. *J Med Chem* **53:**8441-8460.

Rashidi MR and Soltani S (2017) An overview of aldehyde oxidase: an enzyme of emerging importance in novel drug discovery. *Expert Opin Drug Discov* **12:**305-316.

Sanoh S, Horiguchi A, Sugihara K, Kotake Y, Tayama Y, Ohshita H, Tateno C, Horie T, Kitamura S, and Ohta S (2012) Prediction of in vivo hepatic clearance and half-life of drug candidates in human using chimeric mice with humanized liver. *Drug Metab Dispos* **40:**322-328.

Scotcher D, Billington S, Brown J, Jones CR, Brown CDA, Rostami-Hodjegan A, and Galetin A (2017) Microsomal and Cytosolic Scaling Factors in Dog and Human Kidney Cortex and Application for In Vitro-In Vivo Extrapolation of Renal Metabolic Clearance. *Drug Metab Dispos* **45:**556-568.

Sharma R, Strelevitz TJ, Gao H, Clark AJ, Schildknegt K, Obach RS, Ripp SL, Spracklin DK, Tremaine LM, and Vaz AD (2012) Deuterium isotope effects on drug pharmacokinetics. I. System-dependent effects of specific deuteration with aldehyde oxidase cleared drugs. *Drug Metab Dispos* **40:**625-634.

Sodhi JK, Wong S, Kirkpatrick DS, Liu L, Khojasteh SC, Hop CE, Barr JT, Jones JP, and Halladay JS (2015) A novel reaction mediated by human aldehyde oxidase: amide hydrolysis of GDC-0834. *Drug Metab Dispos* **43:**908-915.

Strelevitz TJ, Orozco CC, and Obach RS (2012) Hydralazine as a selective probe inactivator of aldehyde oxidase in human hepatocytes: estimation of the contribution of aldehyde oxidase to metabolic clearance. *Drug Metab Dispos* **40:**1441-1448.

Tan WK, Tan ARY, Sivanandam P, Goh EJH, Yap ZP, Saburulla NF, Austin-Muttitt K, Mullins JGL, and Lau AJ (2020) In Vitro Inhibition of Human Aldehyde Oxidase Activity by Clinically Relevant Concentrations of Gefitinib and Erlotinib: Comparison with Select Metabolites, Molecular Docking Analysis, and Impact on Hepatic Metabolism of Zaleplon and Methotrexate. *J Pharmacol Exp Ther* **374:**295-307.

Terao M, Romao MJ, Leimkuhler S, Bolis M, Fratelli M, Coelho C, Santos-Silva T, and Garattini E (2016) Structure and function of mammalian aldehyde oxidases. *Arch Toxicol* **90:**753-780.

Uehara S, Yoneda N, Higuchi Y, Yamazaki H, and Suemizu H (2020) Human Aldehyde Oxidase 1-Mediated Carbazeran Oxidation in Chimeric TK-NOG Mice Transplanted with Human Hepatocytes. *Drug Metab Dispos* **48:**580-586.

Xie J, Saburulla NF, Chen S, Wong SY, Yap ZP, Zhang LH, and Lau AJ (2019) Evaluation of Carbazeran 4-Oxidation and O (6)-Benzylguanine 8-Oxidation as Catalytic Markers of Human Aldehyde Oxidase: Impact of Cytosolic Contamination of Liver Microsomes. *Drug Metab Dispos* **47:**26-37.

Zientek M, Jiang Y, Youdim K, and Obach RS (2010) In vitro-in vivo correlation for intrinsic clearance for drugs metabolized by human aldehyde oxidase. *Drug Metab Dispos* **38:**1322-1327.

Footnotes

Financial Disclosure: This work received no external funding.

Declaration of interest: The authors report no conflicts of interest.

Legend for Figures

Figure 1. Metabolism of carbazeran to 4-oxo-carbazeran by AOX.

Figure 2. The AOX modulated activity model describes product P formation from substrate S by enzyme E through the formation of the enzyme-substrate complex (ES), which also leads to the formation (k_{inact}) of a less catalytically active version of the enzyme E* ($k_{cat,slow} < k_{cat,fast}$). The substrate and enzyme binding (k_{on}) and dissociation (k_{off}) rate constants are unaffected by the change in the enzyme's catalytic activity.

Figure 3. Time course of carbazeran depletion and 4-oxo-carbazeran formation in liver S9 fraction after incubation with 1 μM carbazeran (A). Time course of 4-oxo-carbazeran formation after incubation with 1 μM (blue), 3 μM (red), 10 μM (yellow), 30 μM (purple) carbazeran in liver (B), kidney (C), lung (D), vasculature (E), and intestinal (F) S9 fractions. Points represent average data with error bars representing standard errors associated with technical and biological (vasculature only) replicates. The curves show AOX modulated activity model simulations based on simultaneous fit to 4-oxo-carbazeran time course data from all tissue S9 fractions.

Figure 4. Formation of 4-oxo-carbazeran in liver (A), kidney (B), lung (C), vasculature (D), and intestinal (E) S9 fractions after 90 minutes of incubation with 1, 3, 10, and 30 μM carbazeran in absence (■) and presence (□) of 100 μM hydralazine.

26

Table 1: **Physiological parameters used for scaling CL$_{int}$ and estimating CL$_{AOX}$ contributions**

Tissue	mg S9 protein / g tissue	g tissue / kg BW	Q$_b$ (mL/min/kg)	References
Liver	120	21.4	20.7	(Zientek et al., 2010; Cubitt et al., 2011)
kidney	39[a]	4.6[a]	16.4	(Obach et al., 2006; Scotcher et al., 2017)
lung	28[a]	10.4[a]	77.9	(Myers et al., 2011; Levitzky, 2013; Scotcher et al., 2017)
Vasculature	8.5[b]	14.3	n/a	(Aird, 2005; Myers et al., 2011)
intestine	27[a]	1.1[a,c]	3.54	(Obach et al., 2006)

n/a = not applicable

[a]personal communication from XenoTech, LLC

[b]personal communication from BioIVT

[c]based on total wet weight of eluted enterocytes

Table 2: Modulated Activity Model (MAM) parameter estimates

Parameter	Liver	Kidney	Lung	Vasculature	Intestine	Units
k_{on}	1.2e8 [3.1e7 - 4.5e8]					μM-1min-1
k_{off}	6.2e8 [1.7e8 - 2.3e9]		2.4e9 [5.0e8 - 1.2e10]			min-1
$k_{cat,fast}$	167 [125 - 224]					min-1
k_{inact}	0.35 [0.26 - 0.46]	0.16 [0.11 - 0.23]	1.1 [0.77 - 1.5]			min-1
$k_{cat,slow}$	4.5 [2.6 - 7.6]	25 [17 - 38]	6.9 [5.2 - 9.2]			min-1
E_{tissue}	21 [17 - 26]	0.038 [0.028 - 0.050]	0.043 [0.032 - 0.059]	0.072 [0.053 - 0.098]	4.7e-3 [3.4e-3 - 6.5e-3]	pmol/mg S9

Values in brackets represent 95% confidence intervals.

Table 3: Calculated parameters and scaled AOX clearance contributions

Tissue	K_M (μM)	V_{max} (pmol/min/mg S9)	CL_{int} (μL/min/mg S9)	$CL_{int,scaled}$ (mL/min/kg)	Total CL_{AOX} (mL/min/kg)
liver	5.2	3507	670	1721	19
kidney	5.2	6.3	1.2	0.22	0.034
lung	21	7.2	0.35	0.10	0.014
vasculature	21	12	0.58	0.071	0.011
intestine	21	0.78	0.038	0.0011	0.00017

carbazeran   AOX   4-oxo-carbazeran

Figure 1

$$E+S \underset{k_{off}}{\overset{k_{on}}{\rightleftharpoons}} ES \xrightarrow{k_{cat,fast}} E+P$$

$$\downarrow k_{inact}$$

$$E^*+S \underset{k_{off}}{\overset{k_{on}}{\rightleftharpoons}} E^*S \xrightarrow{k_{cat,slow}} E^*+P$$
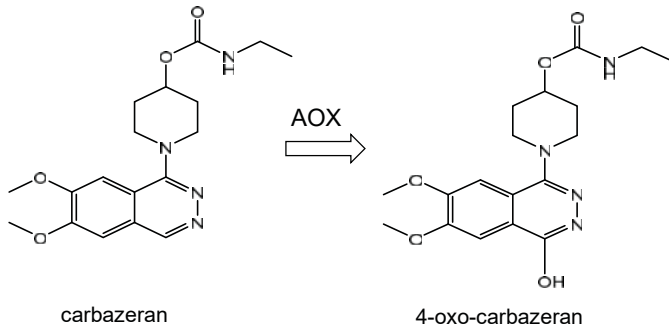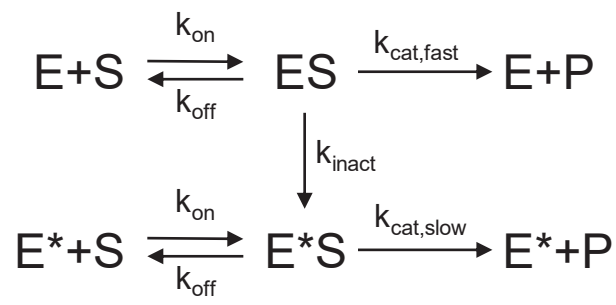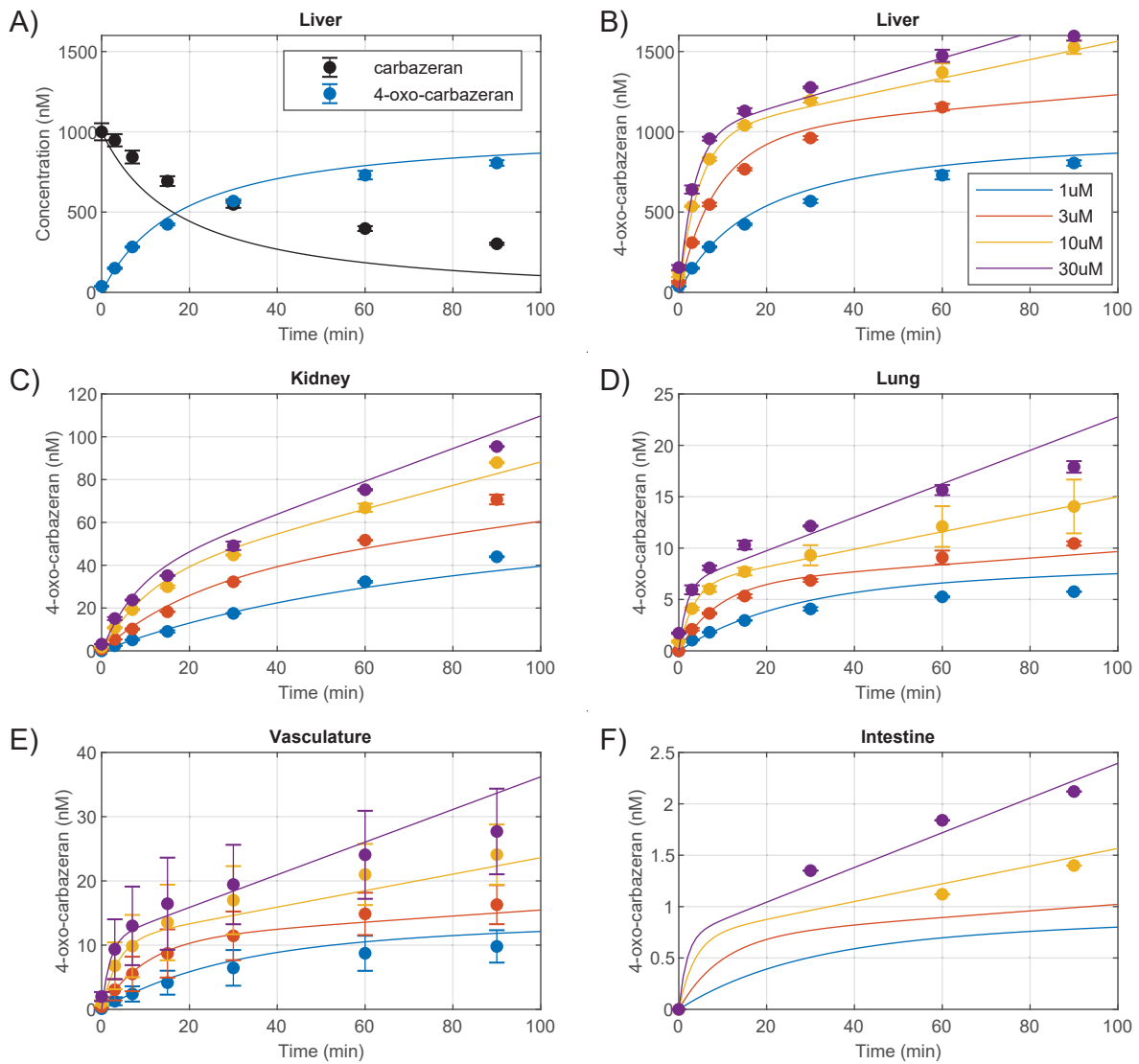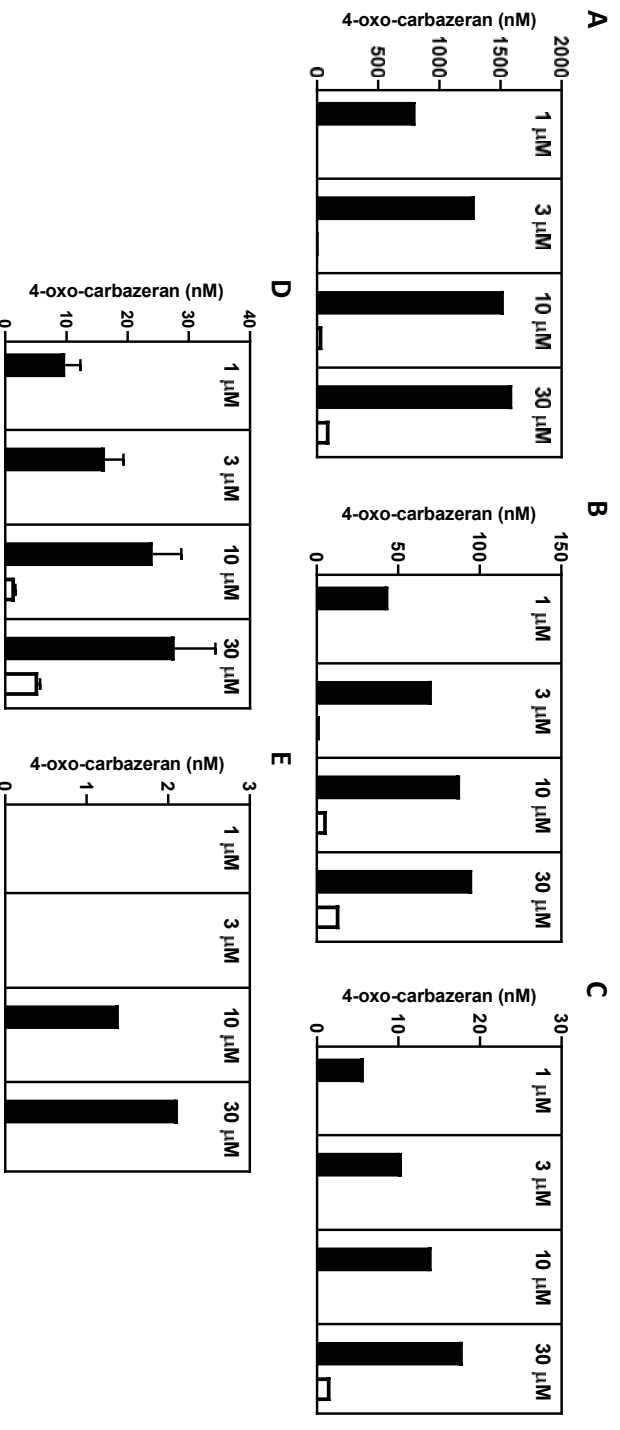
Figure 2

Figure 3

Figure 4

Contribution of extra-hepatic aldehyde oxidase activity to human clearance

Kirk D. Kozminski, Jangir Selimkhanov, Scott Heyward, and Michael A. Zientek

Takeda Pharmaceuticals Limited, San Diego, CA (KDK, JS, MAZ)

BioIVT, Baltimore, MD (SH)

In order to accurately estimate intrinsic clearance using available 4-oxo-carbazeran data, we wanted to precisely capture enzyme activity in each tissue's S9 fraction immediately upon initiation of the reaction with carbazeran. We observed that the rate of 4-oxo-carbazeran formation slowed significantly in all S9 incubations, which Abassi et al., 2019, attributed to inactivation of the AOX enzyme. Thus, to fit the non-linear rate of 4-oxo-carbazeran, we leveraged the AOX modulated activity model (MAM) developed by Abassi et al., 2019. The model (Figure 2) describes product (P) formation from substrate (S) by enzyme (E) through the formation of the enzyme-substrate complex (ES), which also leads to the formation (k_{inact}) of a less catalytically active version of the enzyme E* ($k_{cat,slow}<k_{cat,fast}$). The substrate and enzyme binding (k_{on}) and dissociation (k_{off}) rate constants are unaffected by the change in the enzyme's catalytic activity.

To fit MAM to 4-oxo-carbazeran data across multiple tissues, we initially assumed that all model kinetic parameters were the same across all tissues. This assumption implies that the AOX enzyme activity is unaffected by the potential differences across different tissue milieu. This assumption allows for the estimation of initial active enzyme activity in the intestinal S9 fraction, where product formation was observed only at high substrate concentrations (Figure 3). Additionally, the specific assumption that $k_{cat,fast}$ is the same across all tissue allows us to estimate active enzyme abundances across different tissues. Under this assumption, however, the model was not able to capture liver and kidney 4-oxo-carbazeran time course data sufficiently well (Figure S1).
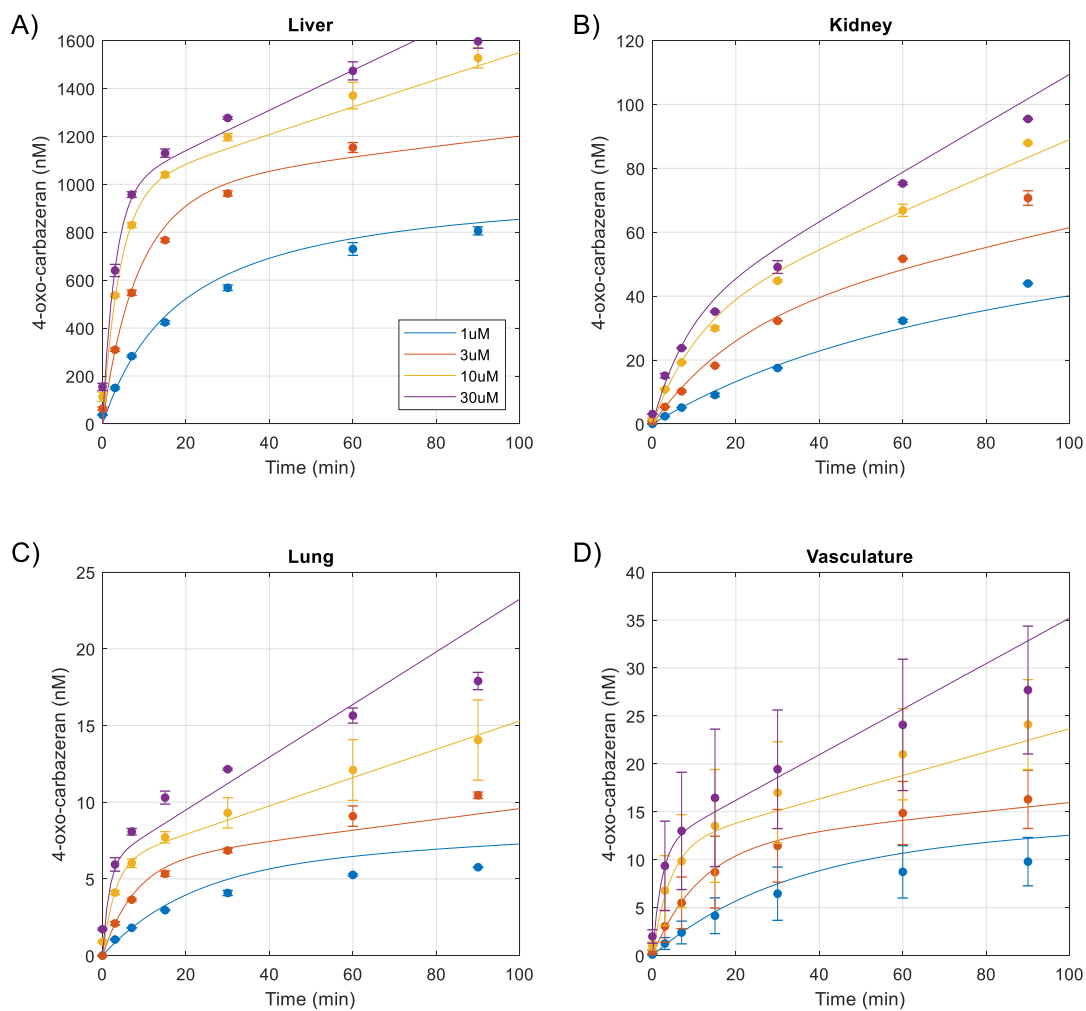
To achieve a better fit to the data, we decided to relax the assumption that all model kinetic parameters had to be the same across all tissues. In order to determine which parameters had to be tissue-specific, we fit each of the well characterized tissues (all excluding intestine due to limited 4-OH formation) independently (Table S1 and Figure S2). We found that K_M, k_{inact}, and $k_{cat,slow}$ for higher substrate-turnover tissues, liver and kidney, were significantly different from those with lower substrate turnover, lung and vasculature. Furthermore, K_M appeared to be similar between kidney and liver. Therefore, we decided to introduce a shared k_{off} ($K_{M,tissue} = \frac{k_{on}+k_{cat,fast}}{k_{off,tissue}}$) parameter specific to liver and kidney as well as liver-specific and kidney-specific k_{inact} and $k_{cat,slow}$ parameters (Table 2). These changes resulted in a much improved model fit to the data (Figure 3), which did not appear significantly different from individual model fits (Figure S2). Based on the Akaike information criterion (AIC), the updated model (AIC = 491) significantly outperformed the initial model (AIC = 609).

**Table S1: Modulated Activity Model individual tissue parameter estimates**

Parameter	Liver	Kidney	Lung	Vasculature	Units
k_{on}	1.1E+07	1.7E+08	6.0E+07	7.9E+07	µM-1min-1
k_{off}	7.3E+07	8.1E+08	1.1E+09	1.5E+09	min-1
$k_{cat,fast}$	252	72	230	119	min-1
k_{inact}	0.42	0.15	1.1	0.88	min-1
$k_{cat,slow}$	6.2	11	9.8	5.1	min-1
E_{tissue}	1.7	0.082	0.031	0.089	pmol/mg S9
K_m	6.8	4.7	19	19	µM
V_{max}	420	5.9	7.1	11	pmol/min/mg S9
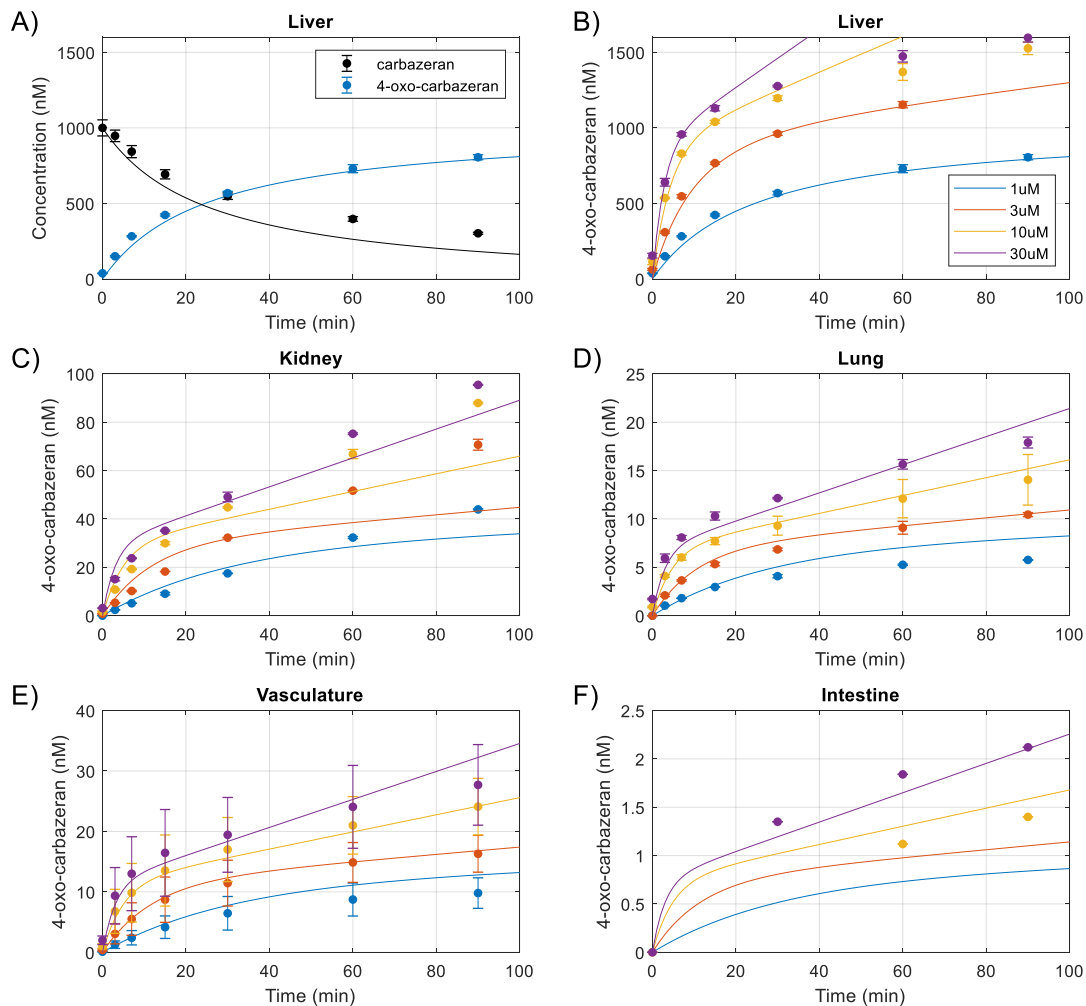
Figure S1. Time course of carbazeran depletion and 4-oxo-carbazeran formation in liver S9 fraction after incubation with 1 µM carbazeran (A). Time course of 4-oxo-carbazeran formation after incubation with 1 µM (blue), 3 µM (red), 10 µM (yellow), 30 µM (purple) carbazeran in liver (B), kidney (C), lung (D), vasculature (E), and intestinal (F) S9 fractions. Points represent average data with error bars representing standard errors associated with technical and biological (vasculature only) replicates. The curves show AOX modulated activity model simulations based on simultaneous fit to 4-oxo-carbazeran time course data from all tissue S9 fractions.

Figure S2. Time course of 4-oxo-carbazeran formation after incubation with 1 μM (blue), 3 μM (red), 10 μM (yellow), 30 μM (purple) carbazeran in liver (A), kidney (B), lung (C), and iliac arterial vasculature (D) S9 fractions. Points represent average data with error bars representing standard errors associated with technical and biological (vasculature only) replicates. The curves show AOX modulated activity model simulations based on simultaneous fit to individual tissue's S9 fraction 4-oxo-carbazeran time course data.
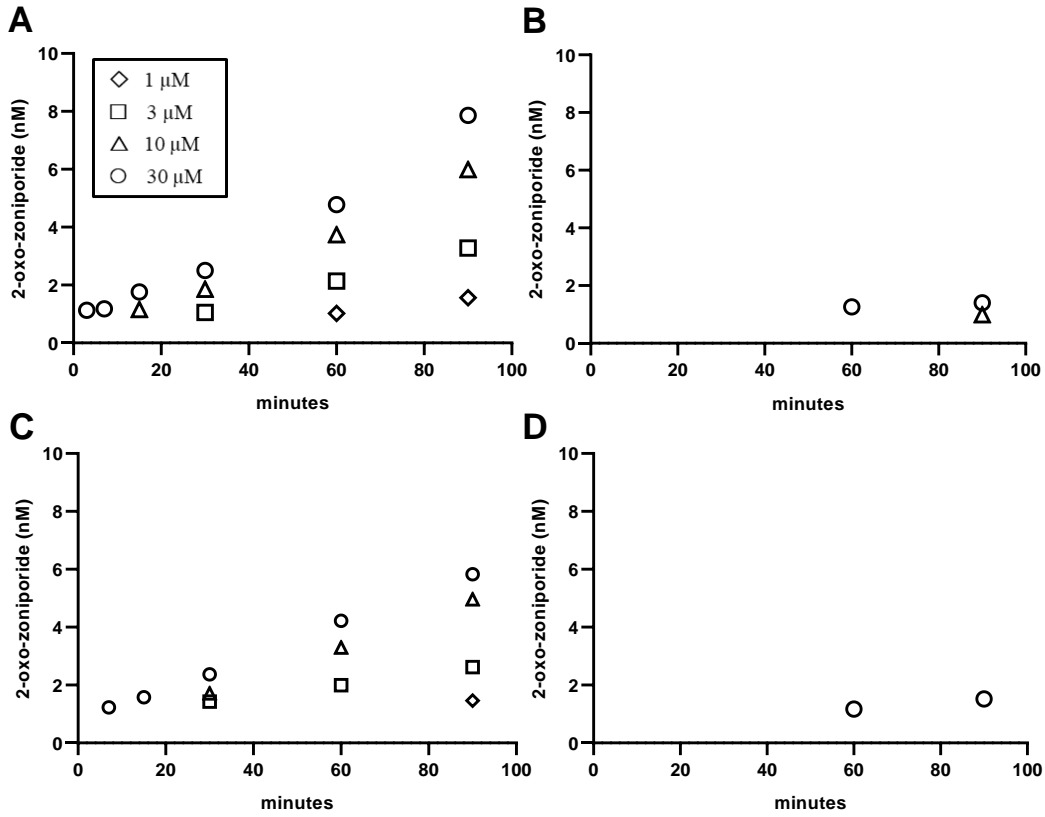
Figure S3. Time course of 2-oxo-zoniporide formation in kidney (A), lung (B), vasculature (C), and intestinal (D) S9 fractions (1 mg/mL) after incubation with 1 μM (◇), 3 μM (□), 10 μM (△), and 30 μM (○) zoniporide.